Electronic Supplementary Material (ESI) for Nanoscale.
This journal is © The Royal Society of Chemistry 2018

SUPPLEMENTARY INFORMATION

Ultralow-Fluence Single-Shot Optical Crystalline-to-Amorphous Phase Transition in Ge-Sb-Te Nanoparticles

Barbara Casarin,[a] Antonio Caretta,[b‡] Bin Chen,[c] Bart J. Kooi,[c] Roberta Ciprian,[b] Fulvio Parmigiani,[a,b,d] and Marco Malvestuto[b]

1 Optical Setup Details

A commercial Coherent Ti:Sapphire regenerative amplified system generates laser pulses with 800 nm central wavelength, of 80 fs duration, and with a repetition rate from 1 kHz to single shot. A BBO non-linear crystal produces second harmonic (400 nm) pulses used to excite the sample, inducing the optical phase-transition. On the contrary, pulses with wavelength equal to the laser fundamental harmonic (800 nm) probes the static transmission of the NPs, before and after the optical phase-transition.

The beam profile is of Gaussian-shape. Knife-edge measurements were used to determine the pump and probe spot-sizes, defined as the $1/e^2$ intensity level. In particular, the p-polarized 400 nm pump beam impinges at normal incidence and is focussed to an elliptical spot with $w_x = 88(2)$ μm and $w_y = 68(2)$ μm. The s-polarized 800 nm probe beam is slightly tilted with respect to the pump angle of incidence and is focussed to a smaller elliptical spot with $w_x = 26(1)$ μm and $w_y = 23(1)$ μm, to ensure transmittivity measurements on an uniformly excited sample area. All the average fluences F_{avg} (mJ/cm^2) considered in this work are defined as the laser pulse energy divided by the $1/e^2$ area of the spot.

[a] *Università degli Studi di Trieste, Via A. Valerio 2, 34127 Trieste, Italy.*
[b] *Elettra-Sincrotrone Trieste S.C.p.A. Strada Statale 14 - km 163.5 in AREA Science Park 34149 Basovizza, Trieste, Italy.*
[c] *Zernike Institute for Advanced Materials University of Groningen, Groningen, 9747 AG, The Netherlands.*
[d] *International Faculty, University of Cologne, 50937 Cologne, Germany.*
‡ Corresponding Author; E-mail: antonio.caretta@elettra.eu

2 Absorbance Spectroscopy Measurements

The absorbance of the NPs was measured using two different optical spectrometers in the visible (VIS) range $300-700$ nm and in the near-infrared (n-IR) range $720-2400$ nm available at the Bio-Lab and at the SISSI beamline at the Elettra Synchrotron facility, respectively. The absorbance, is defined as $A = -\log(T)$, with $T = I/I_0$ the transmittance normalized with respect to the substrate, and ranges from 0 (100% T) to 2 (1% T).

In addition, we explored possible quantum-size effects occurring in our system of $Ge_2Sb_2Te_5$ NPs. The parameter defining the boundary between the bulk and the quantum confinement regimes is the Bohr Exciton Diameter[1]:

$$d_B = 2r_B\varepsilon_{st}/(m^*/m_e) \quad (1)$$

where $r_B = 0.053$ nm is the Bohr Radius, ε_{st} is the static dielectric constant (electronic contribution), m^* is the effective mass and m_e is the bare electron mass. In the case of CdSe nano-crystals, a $\sim 15\%$ band gap increase is observed when dimensions are $d_B/2$.[1] The values for $Ge_2Sb_2Te_5$ ($\varepsilon_{st} = 34.9$[2], $(m^*/m_e) = 0.35$[3]) give $d_B \sim 11$ nm. (A similar value was found for $Ge_1Sb_2Te_4$, i.e. 13 nm[4].) Therefore, in our nanoparticles system ($d < 10.8$ nm) may occur quantum confinement effects, like band gap increasing.

It is important to note that the energy gap in $Ge_2Sb_2Te_5$ is remarkably small (~ 0.38 eV[5,6]). We considered the near IR absorbance spectra (inset of Fig. 2a) and to estimate the band gap in our system we used the Davis-Mott relations[5,6]:

$$(Ah\nu)^{1/2} = C*(h\nu - E_g) \quad (2)$$

where $A = -ln(T/T_{mica})$ is the measured absorbance, C is a con-

stant including the thickness, h is the Plank's constant, ν is the frequency and E_g is the energy gap. Fig. 1 displays the so-called Tauc-plot, where the intercept of the fit with the abscissa gives E_g. In this case, we found $E_g \sim 0.45$ eV, which is roughly 15% higher than that of bulk. In addition, in the low energy region, there is no evidence of other possible confinement effects, like plasmons.

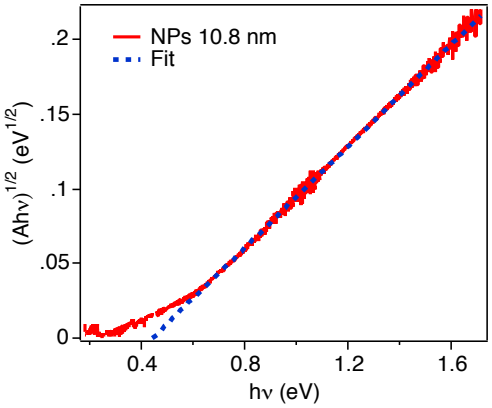

Fig. 1 Tauc plot used for calculating the band gap of $Ge_2Sb_2Te_5$ NPs with 10.8 nm diameter.

3 Optical Microscope Images

The optical microscope images were acquired using an OLYMPUS SZX-system, equipped with a HIGHLIGHT 2100 visible light system, a DP-10 digital camera and a DF PL 2X objective lens.

4 TEM Measurements

Figure 2 shows a bright field HRTEM image of crystalline GST NPs with diameter size 10.8 ± 1.0 nm. The measurement was performed on a JEOL 2010 at 200 kV. Due to the visible high coverage of the substrate (95%), it is possible to note that the NPs can overlap but are distinct between each other. Thus, the sample consists of individual particles. In addition: (i) repeated cycles of single-shot and annealing measurements confirm the constant value of the crystallization temperature at 425 K, and (ii) the statistical transmittivity difference distribution measured over a significant number of single-shot experiments (see Fig. 2(b)) is of symmetric gaussian shape. In fact, coalescence phenomena over subsequent annealings would result in a not-symmetric distribution of the measured transmittivity difference.

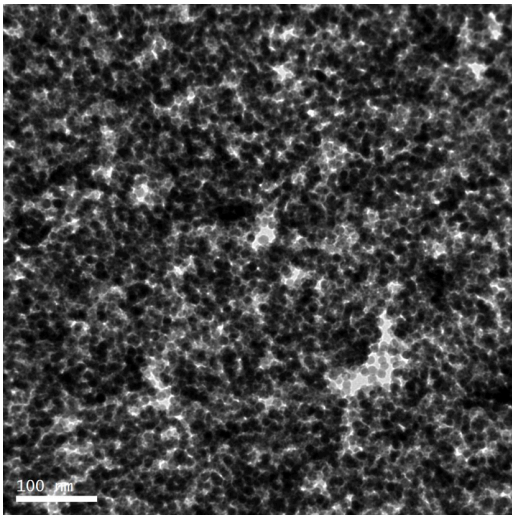

Fig. 2 TEM image of 10.8 ± 1.0 nm $Ge_2Sb_2Te_5$ NPs before the deposition of the PMMA capping layer.

5 Transmittivity Simulations

Our aim is to give a comprehensive explanation of the reduced transmittivity contrast between the crystalline-amorphous NPs. *Nishiuchi et al.*[7] measured the transmittivity in % at 633 nm as a function of increasing temperature of the following system:

- ZnS-SiO2 (30 nm);
- $Ge_2Sb_2Te_5$ (various thickness);
- ZnS-SiO2 (30 nm);
- Glass (0.3 mm);

The values at 75° C and 280° C are representatives of the % transmission of the amorphous and crystalline states, respectively. The transmittivity difference in % between the two states is shown in Figure 3. It is possible to note that the difference in transmission is on the order of 10% around 10 nm, and decreases further with decreasing thickness. We simulated these data with tmm python package, considering the same type of sample stacking and coherent interference. The simulations (dotted and dashed lines in Figure 3) well resemble the data, thus it is a reliable method to account for transmittivity % calculation.

In first approximation, we can consider our system to have the following stacking:

1. PMMA (200 nm);
2. monolayer-like deposited GST NPs embedded in PMMA matrix (various thickness);
3. Mica (0.21 mm)

From *Cohen et al.*[8] we obtained the refractive index of (2): spherical particles, small with respect to wavelength, dispersed in a polarizable insulator dielectric material. Using the same approach, with tmm python package, we calculated the expected transmittivity for this system. The results as a function of the

monolayer-like GST NPs thickness are shown in Figure 4. The red point highlights the value of the absolute transmittivity in % at 10.8 nm, for the crystalline state. This value corresponds roughly to 75%, which is compatible with $T = 10^{-A} = 10^{-0.15} \sim 70\%$, where A is the measured absorbance at 800 nm for crystalline 10.8 nm NPs. The yellow point instead indicates the value of the transmittivity difference in % at 10.8 nm. This value corresponds roughly to 5.5%, which is again compatible with our findings (see Figure 2 in the main text).

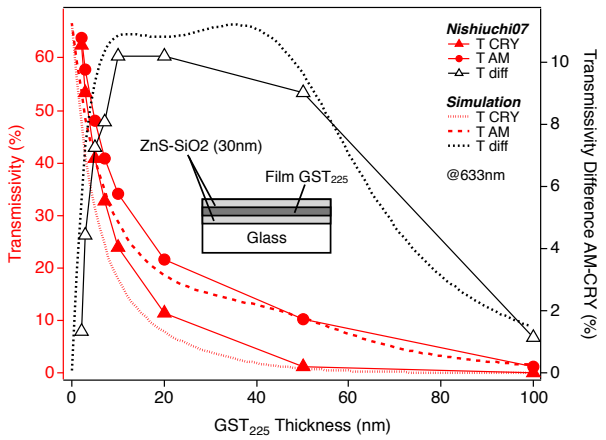

Fig. 3 Experimental and simulated transmittivity and AM-CRY transmittivity difference of a GST thin film with various thickness (from *Nishiuchi et al.*[7]).

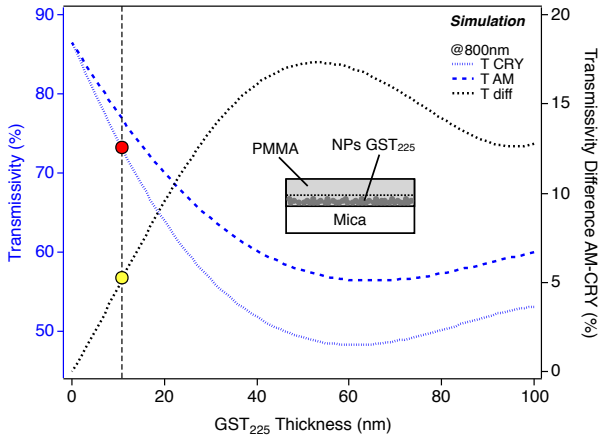

Fig. 4 Simulated transmittivity and AM-CRY transmittivity difference of a monolayer-like deposited GST NPs embedded in PMMA matrix with different thickness.

References

1 A. M. Smith and S. Nie, *Accounts of Chemical Research*, 2010, **43**, 190–200.

2 E. Prokhorov, J. J. Gervacio-Arciniega, G. Luna-Bárcenas, Y. Kovalenko, F. J. Espinoza-Beltrán and G. Trápaga, *Journal of Applied Physics*, 2013, **113**, 113705.

3 J. Kellner, G. Bihlmayer, M. Liebmann, S. Otto, C. Pauly, J. E. Boschker, V. Bragaglia, S. Cecchi, R. N. Wang, V. L. Deringer, P. Küppers, P. Bhaskar, E. Golias, J. Sánchez-Barriga, R. Dronskowski, T. Fauster, O. Rader, R. Calarco and M. Morgenstern, *Communications Physics*, 2018, **1**, 5.

4 T. Siegrist, P. Jost, H. Volker, M. Woda, P. Merkelbach, C. Schlockermann and M. Wuttig, *Nature Materials*, 2011, **10**, 202.

5 E. Vinod, R. Naik, R. Ganesan and K. Sangunni, *Journal of Non-Crystalline Solids*, 2012, **358**, 2927 – 2930.

6 E. M. Vinod, K. Ramesh and K. S. Sangunni, *Scientific Reports*, 2015, **5**, 8050.

7 K. Nishiuchi, N. Yamada, K. Kawahara and R. Kojima, *Japanese Journal of Applied Physics*, 2007, **46**, 7421.

8 R. W. Cohen, G. D. Cody, M. D. Coutts and B. Abeles, *Phys. Rev. B*, 1973, **8**, 3689–3701.